EasyChair Preprint

№ 14770

Granular Scaling Laws for Accurate Prediction of Wheel Mobility on Slopes in Low-Gravity Environments

Takuya Omura and Genya Ishigami

September 9, 2024

9295 | Granular Scaling Laws for Accurate Prediction of Wheel Mobility on Slopes in Low-gravity Environments

Takuya Omura [a,*], Genya Ishigami [a]

[a] *Department of Mechanical Engineering, Keio University, Yokohama, Kanagawa, Japan*

** Corresponding author: ta_hu823tyann@keio.jp*

A B S T R A C T

Analyzing the mobility of wheeled rovers on loose sand in low-gravity environments remains a significant challenge. Among several experimental techniques, such as parabolic flight and reduced-weight tests, granular scaling laws (GSL) have recently been proposed to predict wheel mobility under low-gravity conditions via earth-gravity tests. Although the GSL accurately predicts wheel mobility on flat terrain in low-gravity environments, its capability to predict wheel mobility on slopes in such environments still needs to be verified. This study developed a GSL and investigated its accuracy in predicting wheel mobility on slopes in low-gravity environments. The discrete element method (DEM) was utilized to test wheel mobility at various slope angles under Earth's gravity. Subsequently, by applying a multiple scaling function, the GSL converted the results from the Earth-gravity tests to predict wheel mobility under lunar gravity. The GSL-based predictions were compared with DEM simulations conducted under lunar gravity conditions. The results indicated that the wheel mobility under lunar gravity predicted by the GSL closely corresponded to that calculated via the DEM. These findings indicate that the GSL can accurately predict wheeled-rover mobility on slopes in low-gravity environments.

Keywords
Granular scaling laws
Wheel mobility prediction
Low gravity
Lunar regolith simulant

1. Introduction

The release of the Global Exploration Roadmap (International Space Exploration Coordinate Group, 2018) has increased interest in space exploration. This roadmap calls for extending beyond traditional scientific expeditions to include missions demonstrating technologies for sustained activities on celestial bodies such as the Moon and Mars. The updated space exploration scenario builds on the success of previous missions and illustrates the importance of robotics. In particular, wheeled rovers have proven to have high mobility efficiency on flat terrains, despite their simple mechanism (Sanguino, 2017). They will continue to be among the most widely used tools in future space exploration. Moreover, missions such as NASA's VIPER (Colaprete, 2021) will explore the Moon's craters for water resources. Therefore, the mobility of the rover must be improved to allow it to travel on loose sands and slopes.

Researchers have analyzed wheel–soil interactions on slopes. Sutoh et al. (2012) and Inotsume et al. (2019) studied wheel mobility on slopes with various wheel designs and grousers. Du et al. (2018) and Watanabe et al. (2023) improved terramechanics models by considering soil deformation. However, the effects of gravity were not considered. Therefore, modeling wheel–soil interactions on slopes in low-gravity environments remains an open problem.

The similarity law is valuable for rover design because it can predict wheel mobility under low-gravity conditions through Earth-gravity tests (Kuroda et al., 2005; Li et al., 2012). Slonaker et al. (2017) recently proposed granular scaling laws (GSL) that account for time scaling and employ multiple dimensionless numbers. Thoesen et al. (2020a, 2020b) and Daca et al. (2022, 2023) verified that the GSL accurately predicts wheel mobility on flat terrain in low-gravity environments. Furthermore, Zhang et al. (2020) proposed an expanded GSL for predicting the slope wheel mobility and verified its effectiveness for environments with stronger gravity than Earth.

In the present study, we simulated wheel mobility under various driving conditions in a low-gravity environment and evaluated the prediction accuracy of a developed GSL that combines the concepts proposed by Zhang et al. (2020) and Daca et al. (2022, 2023). Wheel mobility was tested at various slope angles under Earth's gravity using the discrete element method (DEM). The proposed GSL then converted the Earth-gravity test results to predict wheel mobility under lunar gravity. Subsequently, the GSL-based predictions were compared with the results of DEM simulations under lunar gravity conditions. The wheel mobilities under lunar gravity predicted by the GSL closely agreed with those calculated via the DEM. This study contributes to the field of planetary rover mobility in several ways.

- The proposed GSL was comprehensively verified under various driving conditions. The results confirmed the applicability of the GSL for predicting wheel mobility on slopes in a low-gravity environment.
- This study confirmed that the GSL can accurately predict wheel mobility under various slip conditions. In particular, this study is the first to verify the high accuracy of GSL prediction under negative slip ratios, demonstrating the applicability of the GSL even under previously untested and challenging conditions.
- The findings also confirmed the capability of the GSL for predicting time-series data, including transient states. Further, the GSL can accurately predict the power consumption for the rover driving, which is essential for planning and managing their operational time.

https://doi.org/10.56884/ABCD1234 *(ed. note: ISTVS will update your paper's DOI)*
ISBN 978-1-942112-57-0

The remainder of this paper is organized as follows. Section 2 describes the GSL theory and related works. Section 3 presents the numerical experimental methods using the DEM and the simulation setup. In Section 4, the simulation results are presented, the prediction accuracy is evaluated, and the effectiveness of the GSL is demonstrated. Finally, Section 5 concludes the paper and suggests directions for future research.

2. Granular Scaling Laws

Slonaker et al. (2017) derived the original GSL inspired by dynamical similarity in fluid mechanics. The foundational concept of GSL is to provide a physical basis for directly relating different granular locomotion problems for the same soil without additional experiments or simulations, as shown in Fig. 1. Importantly, the GSL is a similarity law that explicitly addresses gravitational acceleration. Therefore, it is a powerful tool for space exploration because it can predict the dynamic behavior of rovers in different gravitational environments. The original GSL is a similarity law composed of multiple dimensionless numbers, as expressed by Eq. 1.

$$\left[\frac{V}{\sqrt{Dg}}, \frac{P}{Mg\sqrt{Dg}}\right] = \Psi_1\left(\sqrt{\frac{g}{D}}t, f, \frac{g}{D\omega^2}, \frac{\rho BD^2}{M}\right) \quad (1)$$

Here, Ψ_1 is a function formulated in dimensionless variables with four inputs and two outputs. Among the output variables, V represents the wheel's horizontal velocity; P represents the power consumed to drive the wheel; and g represents the gravitational acceleration. The wheel parameters M, D, and B represent the mass, diameter, and width, respectively; f is a set of points defining the wheel shape; ω represents the wheel's angular velocity; ρ represents the soil density; and t represents time.

Assuming the same wheel shape f and the same soil, and the test input condition is given as (g, M, D, B, ω), then the other test should be conducted under the condition $(g', M', D', B', \omega') = \left(\alpha g, \beta M, \gamma D, \beta\gamma^{-2}B, \alpha^{1/2}\gamma^{-1/2}\omega\right)$ for any positive scalars α, β, and γ. Correspondingly, the outputs V and P scale such that $(V', P') = \left(\alpha^{1/2}\gamma^{1/2}V, \alpha^{3/2}\beta\gamma^{1/2}P\right)$. In addition, the time at prediction is scaled by $\alpha^{1/2}\gamma^{-1/2}$ because the dimensionless time term is $\sqrt{g/D}\,t$. Thus, Eq. 1 is a similarity law that considers the gravity timescale. Slonaker et al. (2017) verified that two outputs could be accurately predicted under low-speed driving conditions.

Thoesen et al. (2020a, 2020b) and Daca et al. (2022, 2023) enhanced the original GSL. Thoesen et al. (2020a, 2020b) confirmed that the GSL could predict the dynamics of an entire vehicle through coupled multibody dynamics and DEM simulations. Daca et al. (2022, 2023) proposed a GSL with three outputs, which is expressed by Eq. 2.

$$\left[\frac{F_{DP}}{Mg}, \frac{h}{D}, \frac{P}{Mg\sqrt{Dg}}\right] = \Psi_2\left(\sqrt{\frac{g}{D}}t, f, \frac{g}{D\omega^2}, \frac{\rho BD^2}{M}, \frac{V}{\sqrt{Dg}}\right) \quad (2)$$

Here, Ψ_2 is a function with five inputs and three outputs. F_{DP} represents the drawbar pull, and h represents the wheel sinkage. The horizontal velocity of the wheel was controlled to achieve steady slip ratios; thus, the dimensionless number for the velocity V could be moved to the input side. Their contribution was to increase the number of physical quantities that could be predicted and confirm that dimensionless numbers could be moved to either the input or output side.

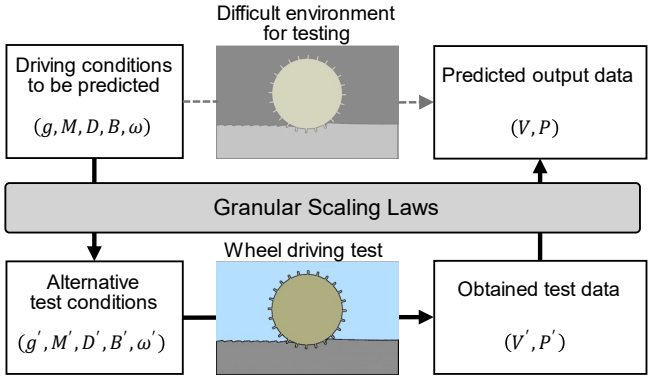

Fig. 1. Conceptual diagram of the original Granular Scaling Laws

Furthermore, Zhang et al. (2020) added the slope angle of the terrain to the input side of Eq. 1, as given by Eq. 3.

$$\left[\frac{V}{\sqrt{Dg}}, \frac{P}{Mg\sqrt{Dg}}\right] = \Psi_3\left(\sqrt{\frac{g}{D}}t, f, \frac{g}{D\omega^2}, \frac{\rho BD^2}{M}, \theta\right) \quad (3)$$

Ψ_3 is a function with five inputs and two outputs, and θ represents the slope angle. Quasi-three-dimensional DEM simulations were used to verify that Eq. 3 is valid for driving conditions in which the slip ratio is >0.5. Note that the gravitational acceleration exceeds that of the Earth.

In this paper, an enhanced GSL is proposed, as expressed by Eq. 4, that combines the concepts in Eqs. 2 and 3 to predict various wheel mobilities during driving on slopes in low-gravity environments.

$$\left[\frac{V}{\sqrt{Dg}}, s, \frac{h}{D}, \frac{P}{Mg\sqrt{Dg}}\right] = \Psi_4\left(\sqrt{\frac{g}{D}}t, f, \frac{g}{D\omega^2}, \frac{\rho BD^2}{M}, \theta\right) \quad (4)$$

Here, Ψ_4 is a function with five inputs and four outputs, and s represents the slip ratio. The slip ratio is strongly correlated with the wheel's horizontal velocity V. However, this ratio is included as one of the output terms because it is a crucial parameter for evaluating wheel mobility in terramechanics. Assuming the same wheel geometry f and the same soil, if the wheel driving data are predicted in the condition $(g, M, D, B, \omega, \theta)$, the experiment should be conducted in the condition $(g', M', D', B', \omega', \theta') = \left(\alpha g, \beta M, \gamma D, \beta\gamma^{-2}B, \alpha^{1/2}\gamma^{-1/2}\omega, \theta\right)$. Then, the output data of interest, such as (V, s, h, P), can be predicted as $\left(\alpha^{-1/2}\gamma^{-1/2}V', s', \gamma^{-1}h', \alpha^{-3/2}\beta^{-1}\gamma^{-1/2}P'\right)$ using the obtained experimental data (V', s', h', P') and the positive scalars α, β, and γ.

3. Numerical method

3.1. Analysis method

The DEM is a numerical simulation method that models granular materials as a collection of discrete particles. By solving for the motion of individual particles at each instant, it allows the analysis of the overall behavior of granular materials and the particle–particle and particle–wheel interactions under various gravity conditions. In this study, the commercial software ANSYS Rocky (ANSYS Inc., 2023) was used to acquire wheel-driving data in low-gravity environments and evaluate the prediction accuracy of the GSL for wheel mobility.

For the force models governing the interactions between particles and between particles and a wheel, the Hertzian spring–dashpot and the Mindlin–Deresiewicz models were adopted for the normal and tangential directions, respectively. These models accurately simulate the dynamic responses of granular materials because they are nonlinear spring–dashpot systems. In addition to these fundamental force models, a rolling resistance model was introduced to simulate the actual shape of a granular material and its resistance to rotation. This made the simulation more realistic by accounting for the intrinsic characteristics of real-world particles. Particles are subject to attractive forces such as van der Waals and electrostatic forces. The DEM can collectively model these forces as adhesive forces. This study adopted a constant-adhesive force model.

Furthermore, the ANSYS DEM provides coarse-grained modeling (CGM), as proposed by Bierwisch et al. (2009), to increase computational efficiency. The CGM reduces the total number of particles in the simulation by representing groups of small particles as larger particles, which are known as parcels. It involves scaling up each parcel using a specific factor referred to as f_{CGM}, which helps maintain the overall system dynamics. The scaling process adjusts the contact and adhesive models to ensure that the dynamics of the scaled-up system are consistent with those of the original particle system. These modifications are made using only the scaling factor, f_{CGM}, to eliminate the need to recalibrate the models. This approach allows efficient simulations while preserving the essential dynamics and interactions observed in the original system. Appendix A details the modeling aspect.

3.2. DEM parameters

The sand with characteristics of a lunar regolith simulant called FJS-1 was considered. Ozaki et al. (2023) measured the characteristics of FJS-1 and found moderate cohesion (Table 1). The DEM parameters were tuned such that the minimum bulk density and direct shear tests performed using the DEM reproduced the characteristics of FJS-1 (Table 1).

The DEM parameters used to reproduce the characteristics of FJS-1 are listed in Table 2. The particle density was considered as a fixed DEM parameter of 2.890 g/cm^3, which was the measured value of FJS-1, and the particle diameter was set to the average grain size of FJS-1. A scaling factor, $f_{\mathrm{CGM}} = 6$, was used during the calibration to reproduce the characteristics of FJS-1. For computational efficiency, a particle size of $f_{\mathrm{CGM}} = 15$ was used in the wheel mobility analysis, which maintained the same driving data as $f_{\mathrm{CGM}} = 6$.

3.3. Wheel design and soil bed

A rigid grouser wheel was used to examine the effectiveness of the GSL. Figure 2 shows the properties of the wheels. The wheel size was the same as that used by Kobayashi et al. (2010) in their parabolic flight experiments, with a wheel diameter D of 150 mm and width B of 80 mm. In addition, the wheel model was designed with 24 grousers of 8.5 mm height to increase the traction force, based on Inotsume et al. (2019). The thickness of the grousers was 2.0 mm. Furthermore, the sandbox was 2400 mm long, 200 mm wide, and 300 mm deep to provide sufficient travel length and neglect the effect of the sandbox walls. The slope angle θ was set by inclining the entire sandbox, as shown in Fig. 2.

Table 1
FJS-1 soil characteristics and soil test results of the discrete element method

Parameter	Measurement results (Ozaki et al., 2023)	DEM soil test results
Minimum bulk density [g/cm^3]	1.549–1.560	1.554
Peak cohesion [kPa]	2.5 (Dr 70%)	2.1
Peak internal friction angle [°]	44.1 (Dr 70%)	43.0
Residual cohesion [kPa]	0.2–1.9	1.0
Residual internal friction angle [°]	34.1–37.2	36.0

Table 2
Discrete element method parameters for FJS-1

Density [g/cm^3]		2.890
Particle diameter [μm]		236 (sphere)
Scaling factor f_{CGM} [-]		6 (soil test calibration) 15 (wheel driving simulation)
Young's modulus [GPa]		0.150
Poisson's ratio [-]		0.30
Rolling resistance coefficient [-]		0.40
	Particle–particle	Particle–wheel
Static friction coefficient [-]	0.40	0.50
Dynamic friction coefficient [-]	0.40	0.50
Restitution coefficient [-]	0.60	0.30
Adhesion coefficient [-]	1.0	0.0
Distance threshold [μm]	5.0	0.0

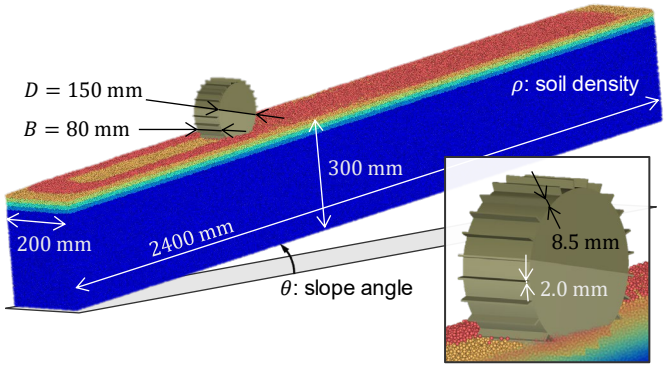

Fig. 2. Wheel properties and slope terrain simulation overview

4. GSL-based prediction results for wheel mobility

10 driving conditions comprising two different angular velocities ω and five different slope angles θ were tested. The predicted targets were the wheel mobilities in lunar gravity (i.e., 1/6 of the Earth's gravity). The test and experimental conditions for Earth's gravity obtained from Eq. 4 are listed in Table 3.

High wheel angular velocities were considered to verify that the GSL can predict wheel mobility even under dynamic conditions, that is, when sand behavior is complex. In addition, rovers used in future planetary explorations will be faster from the perspective of exploratory efficiency. Agarwal et al. (2021) observed that while a linear relationship between the wheel's horizontal velocity and wheel angular velocity is maintained in the quasi-static domain for $\omega < \pi$ rad/s, this proportionality does not hold at higher angular velocities. Therefore, this study defined $\omega \geq \pi$ rad/s as the dynamic domain and selected π and 2π rad/s from this domain.

Table 3
Simulation conditions scaled with scalars $\alpha = 6$, $\beta = 1$, and $\gamma = 1$ based on granular scaling laws

	Gravity g [m/s^2]	Mass M [kg]	Wheel diameter D [mm]	Wheel width B [mm]	Wheel angular velocity ω [rad/s]	Slope angle θ [°]
Predicted targets	1.635	10.2309	150	80	$\{\pi, 2\pi\}$	$\{0, \pm5, \pm10\}$
Experimental conditions under Earth's gravity	9.810	10.2309	150	80	$\{\sqrt{6}\pi, 2\sqrt{6}\pi\}$	$\{0, \pm5, \pm10\}$

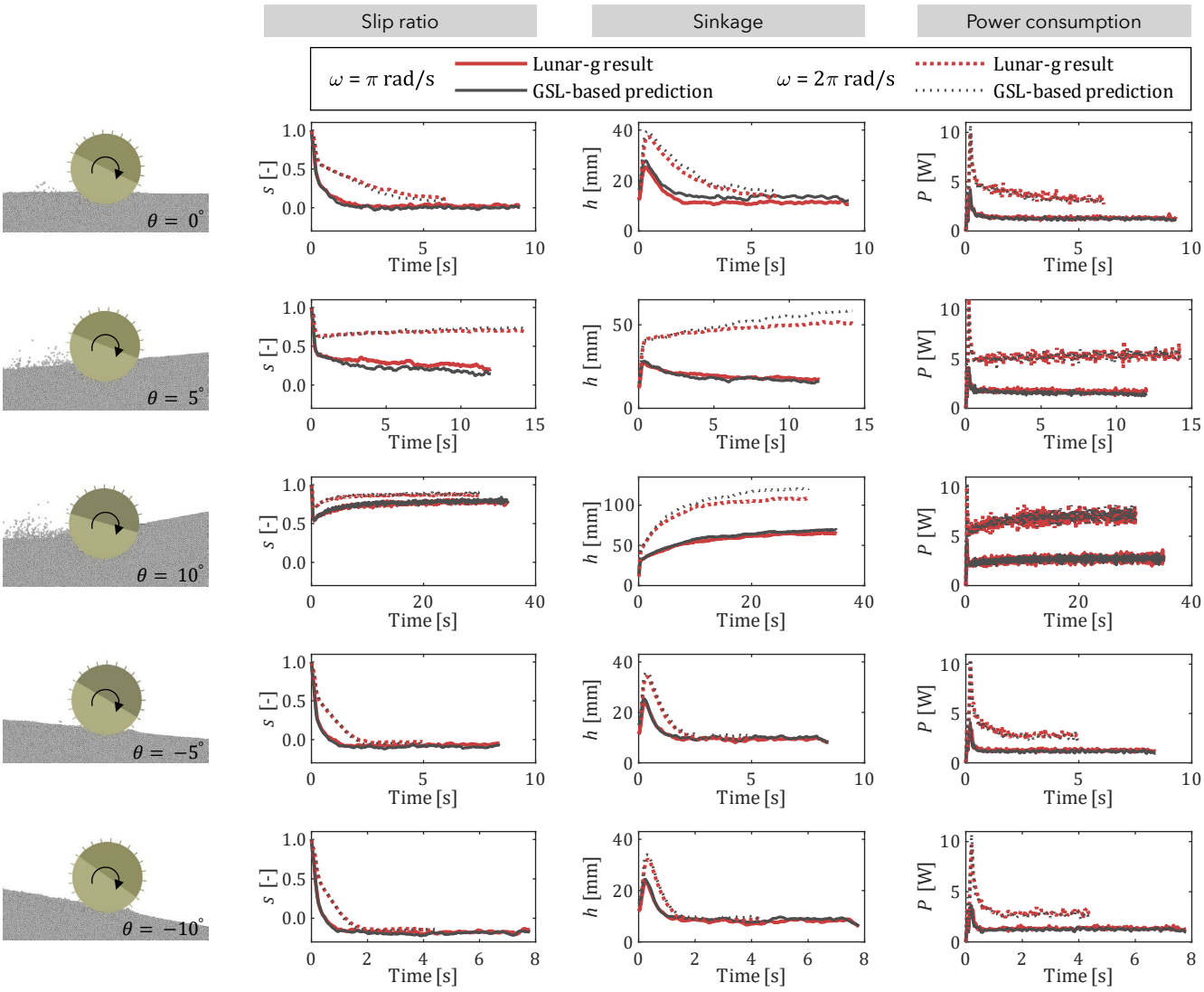

Fig. 3. Simulation results for the wheel driving on various slopes

Figure 3 shows the simulation results at slope angles ranging from -10° to 10°. The red lines represent the wheel mobilities when the wheel is driven under lunar gravity, and the black lines represent the predicted wheel mobilities under lunar gravity based on the GSL from the results obtained under Earth's gravity. Therefore, the black lines represent the converted results of the data (V', s', h', P') from the Earth-gravity tests based on Eq. 4. The results for the wheel's horizontal velocity V are presented in Appendix B owing to space limitations.

The results in Fig. 3 indicate that the GSL can accurately predict the wheel mobilities on slopes in a low-gravity environment, including the slip ratio s, wheel sinkage h, and power consumption P, regardless of the slope angle and wheel angular velocity. The wheel experienced a slip ratio of approximately 0.9 when climbing a 10° slope at a wheel angular velocity of 2π rad/s. Moreover, the wheel experienced a slip ratio of approximately -0.2 when descending a 10° slope at a wheel angular velocity of π rad/s. This suggests that the GSL can accurately predict wheel mobility even under high or negative slip ratio conditions, which can complicate wheel–soil interactions (Johnson et al., 2017). It is particularly noteworthy that the GSL accurately predicts the transient states that begin at the start of wheel driving and settle down to a steady state. This is the first study in which the GSL predictability was determined in transient states, as the DEM provides a stable gravity environment for verification.

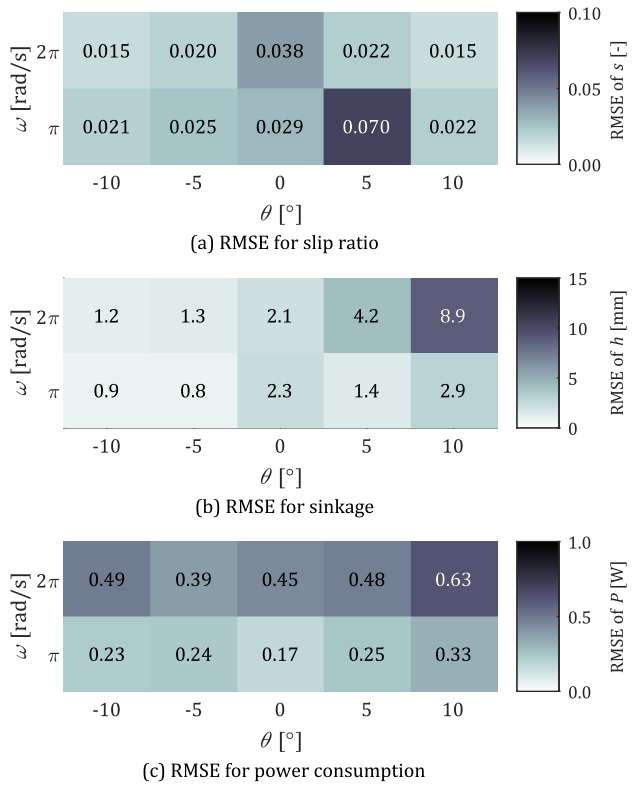

(a) RMSE for slip ratio

(b) RMSE for sinkage

(c) RMSE for power consumption

Fig. 4. Accuracy evaluation of granular scaling laws based on root-mean-square error (RSME)

Figure 4 shows a comparison of the root-mean-square error (RMSE) values for the lunar-g results and the predictions based on the GSL. Fig. 4(a) confirms that the GSL has a high prediction accuracy for the slip ratio. The findings show that the RMSE is as small as 0.015 even under the conditions of $\theta = 10^{\circ}$ and $\omega = 2\pi$ rad/s, when the slip ratio is at its highest ($s \approx 0.9$). In addition, the results quantitatively demonstrated that the GSL is effective for predicting wheel mobility on slopes in low-gravity environments because the RMSE values for climbing/descending a slope are lower than those for driving on flat terrain, except for climbing a 5° slope at an angular velocity of π rad/s.

Figure 4(b) shows the RMSE values for wheel sinkage. The error was larger when the wheel climbed slopes at $\omega = 2\pi$ rad/s than when it drove on flat terrain at the same speed. However, the scaled-up grain size was approximately 3.5 mm; thus, the magnitude of the error was a few sand grains. Furthermore, the prediction results of wheel sinkage based on the GSL exceed the lunar-gravity results, as shown in Fig. 3. This indicates that the GSL tends to predict worse performance than actual observations, thus providing a margin of safety. Such conservative estimates are beneficial in designing wheel systems and planning rover missions. This conservatism of the GSL corresponds with the results verified by Daca et al. (2022, 2023) in their parabolic flight experiments.

Finally, the RMSE values for the power consumed to drive the wheel are presented in Fig. 4(c). The RMSE is larger with a higher angular velocity of the wheel. This is attributed to more power being consumed. The results indicated highly accurate predictions of power consumption at different slopes and wheel speeds.

5. Conclusions and future work

This study simulated the wheel mobilities under various slope angles and wheel angular velocities and evaluated the prediction accuracy to demonstrate the effectiveness of an enhanced GSL that combines the concepts proposed by Zhang et al. (2020) and Daca et al. (2022, 2023). The DEM simulation reproduced sand with soil characteristics similar to those of a lunar regolith simulant to create an environment that closely resembled the actual lunar surface. Subsequently, wheel mobility was tested at slope angles ranging from -10° to 10° under Earth's gravity. In the analysis, the enhanced GSL was applied to convert the Earth-gravity test results to predict the wheel mobility under lunar gravity. These GSL-based predictions were compared with the wheel mobility results obtained from DEM simulations under lunar gravity conditions. The comparison results indicated that the GSL can accurately predict the wheel mobility for the slip ratio, sinkage, and power consumption needed to drive the wheel. In addition, the accuracy of wheel-mobility prediction for sloped driving was comparable to that for flat terrain. These results verify that the GSL effectively predicts the wheel slope-driving performance in low-gravity environments. Additionally, the simulation results demonstrated for the first time that the GSL can be applied over a wide range of slip conditions, from a negative slip ratio of approximately –0.2 to a high slip ratio of approximately 0.9. Furthermore, the simulation results suggest that the GSL can be applied to time-series prediction, including transient states.

Overall, the GSL is an effective method for predicting complex wheel mobility in low-gravity environments, on a wide range of slopes, and at high speeds. Therefore, the GSL is essential for planning and executing space exploration missions. In future work, the prediction accuracy should be investigated when using scaled-down wheels to increase the cost efficiency of the rover design process.

6. Nomenclature

B	Wheel width	[mm]
D	Wheel diameter	[mm]
f	Wheel shape function	[-]
f_{CGM}	Scaling factor for coarse-grain model	[-]
F_{DP}	Drawbar pull	[N]
g	Gravitational acceleration	[m/s^2]
h	Wheel sinkage	[mm]
M	Wheel mass	[kg]
P	Power consumption to drive a wheel	[W]
s	Slip ratio	[-]
t	Time	[s]
V	Wheel horizontal velocity	[mm/s]
α	Scaling factor for gravitational acceleration	[-]
β	Scaling factor for wheel mass	[-]
γ	Scaling factor for wheel diameter	[-]
θ	Slope angle	[°]
ρ	Soil density	[g/cm^3]
Ψ_1	GSL function of Slonaker et al. (2017)	[-]
Ψ_2	GSL function of Daca et al. (2022, 2023)	[-]
Ψ_3	GSL function of Zhang et al. (2020)	[-]
Ψ_4	GSL function of this study	[-]
ω	Wheel angular velocity	[rad/s]

7. Acknowledgements

This study was partially supported by JSPS KAKENHI (grant number: JP23KJ1901).

8. Declaration of competing interest

The authors declare that they have no competing financial interests or personal relationships that could have influenced the work reported herein.

9. References

Agarwal, S., Karsai, A., Goldman, D. I., Kamrin, K., 2021. Surprising simplicity in the modeling of dynamic granular intrusion. Sci. Adv. 7(17), eabe0631.

Ansys Inc., 2023. DEM technical manual: release 2023 R2.

Bierwisch, C., Kraft, T., Riedel, H., Moseler, M., 2009. Three-dimensional discrete element models for the granular statics and dynamics of powders in cavity filling. J. Mech. Phys. Solids, 57(1), 10-31.

Colaprete, A., 2021. Volatiles investigating polar exploration rover (viper).

Daca, A., Skonieczny, K., 2022. Evaluating 1-G testing methods for Predicting Planetary Rover Mobility in reduced gravity. In 16th Symposium on Advanced Space Technologies in Robotics and Automation (ASTRA) 2022, Noordwijk, The Netherlands.

Daca, A., Tremblay, D., Skonieczny, K., 2023. Expansion and experimental evaluation of scaling relations for the prediction of wheel performance in reduced gravity. Microgravity Sci. Technol. 35, 59.

Du, Y., Gao, J., Jiang, G., Zhang, Y., 2018. Development and numerical validation of an improved prediction model for wheel-soil interaction under multiple operating conditions. J. Terramech. 79, 1-21.

Inotsume, H., Moreland, S., Skonieczny, K., Wettergreen, D., 2019. Parametric study and design guidelines for rigid wheels for planetary rovers. J. Terramech. 85, 39-57.

International Space Exploration Coordination Group, 2018. ISECG Global Exploration Roadmap (3rd edition). https://www.globalspaceexploration.org/wordpress/wp-content/isecg/GER_2018_small_mobile.pdf (accessed 26 March 2024).

Johnson, J. B., Duvoy, P. X., Kulchitsky, A. V., Creager, C., Moore, J., 2017. Analysis of Mars exploration rover wheel mobility processes and the limitations of classical terramechanics models using discrete element method simulations. J. Terramech. 73, 61-71.

Kobayashi, T., Fujiwara, Y., Yamakawa, J., Yasufuku, N., Omine, K., 2010. Mobility performance of a rigid wheel in low gravity environments. J. Terramech. 47, 261-274.

Kuroda, Y., Teshima, T., Sato, Y., Kubota, T., 2005. Mobility performance evaluation of planetary rovers in consideration of different gravitational acceleration. In 2005 IEEE/RSJ International Conference on Intelligent Robots and Systems, pp. 2991-2996.

Li, M., Gao, F., Sun, P., 2012. Prediction method of lunar rover's tractive performance based on similitude methodology. In 2012 Fifth International Conference on Intelligent Computation Technology and Automation, pp. 686-689.

Ozaki, S., Ishigami, G., Otsuki, M., Miyamoto, H., Wada, K., Watanabe, Y., Nishino, T., Kojima, H., Soda, K., Nakao, Y., Sutoh, M., Maeda, T., Kobayashi, T., 2023. Granular flow experiment using artificial gravity generator at International Space Station. NPJ Microgravity 9, 61.

Sanguino, T. D. J. M., 2017. 50 years of rovers for planetary exploration: A retrospective review for future directions. Robot. Auton. Syst. 94, 172-185.

Sutoh, M., Yusa, J., Nagatani, K., Yoshida, K., 2021. Traveling performance evaluation of planetary rovers on loose soil. J. Field Robot. 29(4), 648-662.

Slonaker, J., Motley, D. C., Zhang, Q., Townsend, S., Senatore, C., Iagnemma, K., Kamrin, K., 2017. General scaling relations for locomotion in granular media. Phys. Rev. E, 95(5), 052901.

Thoesen, A., McBryan, T., Mick, D., Green, M., Martia, J., Marvi, H., 2020a. Comparative performance of granular scaling laws for lightweight grouser wheels in sand and lunar simulant. Powder Technol. 373, 336–346.

Thoesen, A., McBryan, T., Mick, D., Green, M., Martia, J., Marvi, H., 2020b. Granular scaling laws for helically driven dynamics. Phys. Rev. E 102, 032902.

Watanabe, Y., Nakano, S., Suzuki, H., Ozaki, S., 2023. Numerical analysis of wheel locomotion on soft soil using the extended terramechanics model based on cellular automata. J. Terramech. 109, 9-20.

Zhang, Q., Townsend, S., Kamrin, K., 2020. Expanded scaling relations for locomotion in sloped or cohesive granular beds. Phys. Rev. Fluids. 5(11), 114301.

Appendix A. DEM models

In this study, nonlinear spring-dashpot models were used as the contact-force models between particles and between particles and a wheel. The Hertzian spring-dashpot model was considered for the normal contact force F_n, as expressed by Eq. (A.1).

$$F_n = k_n s_n^{\frac{3}{2}} + c_n s_n^{\frac{1}{4}} \dot{s_n} \tag{A.1}$$

Here, k_n and c_n represent the normal contact stiffness and damping coefficient, respectively. s_n represents the contact normal overlap, and $\dot{s_n}$ represents the time derivative of the contact normal overlap.

The Mindlin–Deresiewicz model calculates the tangential force F_τ given by Eq. (A.2).

$$F_\tau = -k_\tau F_n \left(1 - \varsigma^{\frac{3}{2}}\right) + c_\tau F_n^{\frac{1}{2}} \varsigma^{\frac{1}{4}} \dot{s_\tau} \tag{A.2}$$

$$\varsigma = 1 - \frac{\min\left(s_\tau,\ s_{\tau,\max}\right)}{s_{\tau,\max}} \tag{A.3}$$

Here, k_τ and c_τ represent the tangential contact stiffness and the normal damping coefficient, respectively. s_τ represents the tangential relative displacement at the contact, and $\dot{s_\tau}$ represents the tangential component of the relative velocity at the contact. $s_{\tau,\max}$ represents the maximum relative tangential displacement at which particles begin to slide, and ς represents the proportion of acceptable tangential displacement before the particles begin to slide.

An attractive normal force to the repulsive contact force described above was included in the model to represent the cohesive force of sand. A constant-adhesive force model was used. This model is the simplest adhesion model, where a constant force $F_{n,\mathrm{adh}}$ is applied between particles closer than a certain distance δ_{adh}. This model is expressed by Eq. (A.4).

$$F_{n,\mathrm{adh}} = \begin{cases} 0 & \text{if} - s_n \geq f_{\mathrm{CGM}} \delta_{\mathrm{adh}} \\ \dfrac{f_{\mathrm{adh}} mg}{f_{\mathrm{CGM}}} & \text{if} - s_n < f_{\mathrm{CGM}} \delta_{\mathrm{adh}} \end{cases} \tag{A.4}$$

Here, f_{adh} is the adhesion coefficient, and δ_{adh} is the distance threshold determining whether adhesion occurs between particles. m represents the particle mass.

Using a rolling resistance model is practical for reproducing the nonspherical shape of particles and the resistance to rotation caused by this shape. The rolling resistance moment M_τ^t for the linear spring rolling limit used is expressed by Eq. (A.5).

$$M_\tau^t = \min\left(M_r^t, \mu_r \frac{r F_n}{2}\right) \tag{A.5}$$

Here, μ_r is the rolling resistance coefficient, and r represents the rolling radius of the particles. M_r^t is a purely elastic rolling resistance parameter given by Eq. (A.6).

$$M_r^t = M_r^{t-\Delta t} - k_r \omega_{\mathrm{rel}} \Delta t \tag{A.6}$$

Here, $M_r^{t-\Delta t}$ represents the rolling resistance moment at the previous time; k_r represents the rolling stiffness; ω_{rel} represents the relative angular velocity, which is defined as the difference between the angular velocities of two particles in contact; and Δt represents the simulation timestep.

Appendix B. Additional simulation results

Figure B.1 shows a comparison of the wheel's horizontal velocities in lunar gravity and the predicted ones based on the GSL in the DEM simulation. The results indicate that the GSL can accurately predict the horizontal velocity V, as shown in Fig. B.1.

The prediction accuracy for the horizontal velocity is related to that for the slip ratio. The slip ratio s is expressed in terms of the horizontal velocity V and the input angular velocity ω, as given by Eq. (B.1). Therefore, if the GSL accurately predicts the slip ratio s for an appropriately scaled input angular velocity ω', it can also predict the horizontal velocity V correctly. This can be explained by a variant of the equation, as given by Eq. (B.2).

$$s = 1 - \frac{V}{\frac{D}{2}\omega} \tag{B.1}$$

$$\begin{aligned} \frac{V'}{\sqrt{D'g'}} &= \frac{\frac{D'}{2}\omega'(1-s')}{\sqrt{D'g'}} = \frac{\frac{\gamma D}{2}\sqrt{\frac{\alpha}{\gamma}}\omega(1-s)}{\sqrt{\gamma D \alpha g}} \\ &= \frac{\frac{D}{2}\omega(1-s)}{\sqrt{Dg}} = \frac{V}{\sqrt{Dg}} \end{aligned} \tag{B.2}$$

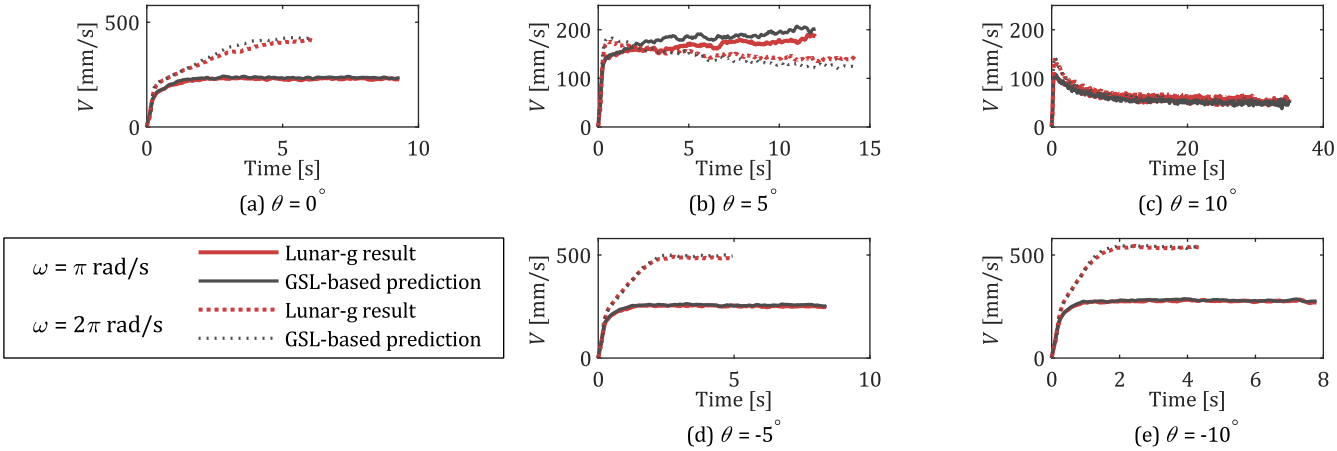

Fig. B.1. Simulation results for the wheel's horizontal velocity